

## Structure, equation of state, diffusion and viscosity of warm dense Fe under the conditions of a giant planet core

Jiayu Dai<sup>1,3</sup>, Yong Hou<sup>1</sup>, Dongdong Kang<sup>1</sup>, Huayang Sun<sup>1</sup>, Jianhua Wu<sup>1</sup> and Jianmin Yuan<sup>1,2,3</sup>

<sup>1</sup> Department of Physics, College of Science, National University of Defense Technology, Changsha 410073, People's Republic of China

<sup>2</sup> State Key Laboratory of High Performance Computing, National University of Defense Technology, Changsha 410073, People's Republic of China

E-mail: [jydai@nudt.edu.cn](mailto:jydai@nudt.edu.cn) and [jmyuan@nudt.edu.cn](mailto:jmyuan@nudt.edu.cn)

*New Journal of Physics* **15** (2013) 045003 (15pp)

Received 2 December 2012

Published 8 April 2013

Online at <http://www.njp.org/>

doi:10.1088/1367-2630/15/4/045003

**Abstract.** Fe exists abundantly in the universe. In particular, the dynamic structures and transport properties of warm dense Fe are crucial for understanding the evolution and structures of giant planets. In this paper, we present the ionic structures, equation of states, diffusion and viscosity of Fe at two typical densities of 33.385 and 45 g cm<sup>-3</sup> in the temperature range of 1–10 eV, giving the data by the first principles calculations using quantum Langevin molecular dynamics. Furthermore, the validation of the Stokes–Einstein (SE) relation in this regime is discussed, showing the importance of choosing the effective atomic diameter. The results remind us of the careful usage of the SE relation under extreme conditions.

<sup>3</sup> Authors to whom any correspondence should be addressed.



Content from this work may be used under the terms of the [Creative Commons Attribution 3.0 licence](https://creativecommons.org/licenses/by/3.0/). Any further distribution of this work must maintain attribution to the author(s) and the title of the work, journal citation and DOI.

**Contents**

<b>1. Introduction</b>	<b>2</b>
<b>2. Methods</b>	<b>3</b>
<b>3. Convergence tests</b>	<b>5</b>
<b>4. Structural dynamics</b>	<b>7</b>
<b>5. Transport properties</b>	<b>8</b>
<b>6. Stokes–Einstein relation</b>	<b>10</b>
<b>7. Conclusion</b>	<b>13</b>
<b>Acknowledgments</b>	<b>13</b>
<b>References</b>	<b>13</b>

**1. Introduction**

The properties of complex materials such as Fe under extreme conditions are crucial for understanding the evolution of planets (Earth, giant planets and extro-solar giant planets) [1] and stars such as the Sun [2, 3]. More interestingly, the laser-driven and Z-pinch experiments can lead to very high densities up to hundreds of  $\text{g cm}^{-3}$  and temperatures up to thousands of eV [4, 5]. In particular, temperatures of 1–10 eV with associated pressures of 10–1000 TPa are likely to exist in the interiors of massive planets [6, 7]. Recent studies have shown the possible stable structures of Fe at these pressures [6, 7], where face-centered cubic (fcc) structures are stable in the range of 7–21 TPa. However, the effect of temperature on these structures is still not known, since the dynamic structures such as melting, diffusion and viscosity can be induced by temperatures; the phases of Fe in Earth-like exoplanets are likely to be liquid. In order to understand these behaviors, since the experimental determination currently seems to be extremely expensive and difficult, accurate simulations are required for the determination of the structures and dynamics. The dynamic structures of Fe and its compounds from first principles molecular dynamics under the physical conditions of the Earth's core have been studied widely [8–10], showing the complexity of the new phenomena in high energy density physics. In particular, it is worth verifying whether the Stokes–Einstein (SE) relation at such high densities is valid, since the SE relation is one important bridge between dynamics and statistics; it has usually been adopted in previous calculations of viscosities from diffusion coefficients [8–12]. Up to now, the diffusion and viscosity can be obtained directly by molecular dynamics simulations with the Kubo–Green relation [10–13]. Moreover, we can construct statistical models according to the simulation results by introducing easy applications in hydrodynamics [14, 15]. However, molecular dynamics simulations are strongly dependent on the accuracy of many-body interatomic potentials; there are usually some limitations to statistical methods.

A cold stable fcc structure, with its inducing liquid at a high temperature, is considered an important phase in giant planets such as Jupiter and exoplanets [6, 7]. In this regime, the densities are from 33.9 to 66.7  $\text{g cm}^{-3}$  and the temperatures are from 1 to 10 eV. For these states, the melting behaviors and the transport properties are interesting and deserve to be studied carefully. Besides, a high density will introduce many different chemical bonds since a pressure greater than 1 Mbar will change the traditional chemistry dramatically [16–20]. Furthermore, when

the pressure increases to 100 Mbar, the core electron charge density can be changed significantly [16–18]. Therefore, the transport properties such as equation of states (EOS), diffusion and viscosity will change a lot since these properties are related to the electronic structures. With respect to the methods of calculating these properties accurately, first principles calculations are thus required because we did not understand their behaviors from semiclassical models, such as the average atom (AA) model [21, 22] and the Thomas–Fermi model or the orbital free method [23–25], in which the orbital behaviors or chemical bonds information cannot be described well.

Molecular dynamics combining the finite-temperature density functional theory (DFT) [26], called quantum molecular dynamics (QMD), and quantum Langevin molecular dynamics (QLMD) have been successfully used in warm and hot dense matter, especially under very high pressures [8, 10, 18–20, 27, 28]. The validations of QMD and QLMD at high densities and temperatures have been verified many times by comparing with experiments and interestingly reasonable results are found. In particular, QMD is considered as one of the most promising methods and has been successfully used to predict the transport properties of warm dense matter (WDM) [29, 31]. The biggest argument against QMD applications is that it limits the number of particles because of its computational cost at high temperature. However, QMD and QLMD can be efficient for the calculations of WDM under the conditions of a giant planet core; they can give relatively accurate transport properties using a few hundred particles [29–32]. In this paper, we adopted QLMD to simulate the transport properties of dense Fe at  $45 \text{ g cm}^{-3}$  from 1 to 10 eV. Except for considering the density of  $33.385 \text{ g cm}^{-3}$  at 100 eV along the Hugoniot curve [18], we also calculate the dynamical properties at  $33.385 \text{ g cm}^{-3}$  up to 10 eV. Furthermore, the approximation of the SE relation is discussed, showing the debatable validation under such dense regimes.

## 2. Methods

For the complexity of Fe at high density, both QMD with the velocity rescaling method and QLMD simulations are tested first. In fact, at low temperatures, the electron–ion collision induced friction is small since the friction is proportional to the temperature. Therefore, QMD and QLMD are equivalent for the equilibrium properties at low temperatures. Eventually, the advantage of QLMD is its higher computational efficiency compared to traditional QMD [33]. The electronic structures are solved based on finite temperature DFT implemented in the Quantum ESPRESSO package [34]. Considering the small atomic sizes at high density, the time step of 0.5 fs is used in order to keep the correct trajectories of ions. The pseudopotential (PP) is one of the key points in QMD and QLMD simulations. Here, we construct a new PP with 16 electrons in the valence and 0.9 atomic units for the radius cutoff within the generalized-gradient approximation [35], which can promise correctness with respect to the conditions we are studying. Using this PP, we can reproduce the bulk modulus properties of Fe as previous results calculated by full-electron calculations and experiments. More importantly [18, 36], at high pressure, the pressure and band structures at the density of 33.9 and  $48.23 \text{ g cm}^{-3}$  are in good agreement with the pressure in [7] using the same PP [18]. Furthermore, the same PP has been successfully used to calculate the EOS of Fe in a hot dense regime within a wide range of densities and temperatures [18], indicating the validation of PP in this work. Besides, 2000 time steps with a large convergent tolerance of  $1.0 \times 10^{-4}$  in electronic structure calculations are adopted in order to reach the thermalization; 10 ps time lengths with a small convergent

tolerance of  $1.0 \times 10^{-6}$  [33] are simulated to obtain the transport properties and thermal average. In order to accelerate the calculations, the Gamma point is only used for the representation of the Brillouin zone. To compare with the results from semiclassical methods, averaged atom molecular dynamics (AAMD) [22, 37] is performed for all cases. When two atoms are close enough, their electronic distributions overlap, inducing interactions between them. In order to describe these interactions, we should establish the interatomic potential. In the AAMD method, the temperature-dependent pair potential, which can describe the contributions of overlapping electronic distributions, is constructed from the AA electronic calculations, including the ionic correlations within the framework of the AA model. Within this framework, the ions are moving on this pair potential, giving the ionic trajectories and ionic configurations at different times. From AAMD, we can basically use a large number of particles and give the convergent results corresponding to the size effects. The comparison between QLMD and AAMD has been reported before [19, 33], showing their agreement at high temperatures. The details of AAMD can be found in [37].

The self-diffusion coefficient  $D$  can be obtained from two methods. One is from the trajectories by the mean-square displacement  $D^R$

$$D^R = \frac{1}{6t} \langle |\mathbf{R}_i(t) - \mathbf{R}_i(0)|^2 \rangle, \quad (1)$$

where the  $\mathbf{R}_i$  is the position of the  $i$ th particle. The other method is from the velocity autocorrelation function  $D^V$

$$D^V = \frac{1}{3} \int_0^\infty \langle \mathbf{V}_i(t) \mathbf{V}_i(0) \rangle dt, \quad (2)$$

where  $\mathbf{V}_i$  is the velocity of the  $i$ th particle. Besides, the viscosity  $\eta$  can be obtained from the autocorrelation function of the off-diagonal component of the stress tensor, the so-called Green–Kubo equation [10, 38]

$$\eta = \lim_{t \rightarrow \infty} \bar{\eta}(t) = \lim_{t \rightarrow \infty} \frac{V}{k_B T} \int_0^t \langle P_{12}(0) P_{12}(t') \rangle dt', \quad (3)$$

where  $P_{12}$  represents the averaged result for the five independent off-diagonal components of the stress tensor  $P_{xy}$ ,  $P_{yz}$ ,  $P_{zx}$ ,  $(P_{xx} - P_{yy})/2$  and  $(P_{yy} - P_{zz})/2$ . Using this method, the self-diffusion coefficient and viscosity of warm and hot dense matter have been reported widely [8–12, 29, 39–42] within the framework of QMD, showing its validation in these extreme conditions.

On the other side, the viscosity can also be calculated directly from the SE relation

$$D\eta = k_B T / (2\pi a), \quad (4)$$

where  $a$  is an effective atomic diameter. This relation is statistically obtained from the Brownian motion of a macroscopic particle in liquid, but it is only an approximation for the atoms. If the validation of the SE relation can be verified, the size of particles and the transport behaviors can be understood well [43]. In fact, for a Brownian particle, the SE relation is equivalent to equations (2) and (3). In particular, for dense matter, the diameters of atoms are very small so the validation of the SE relation should be examined very carefully.

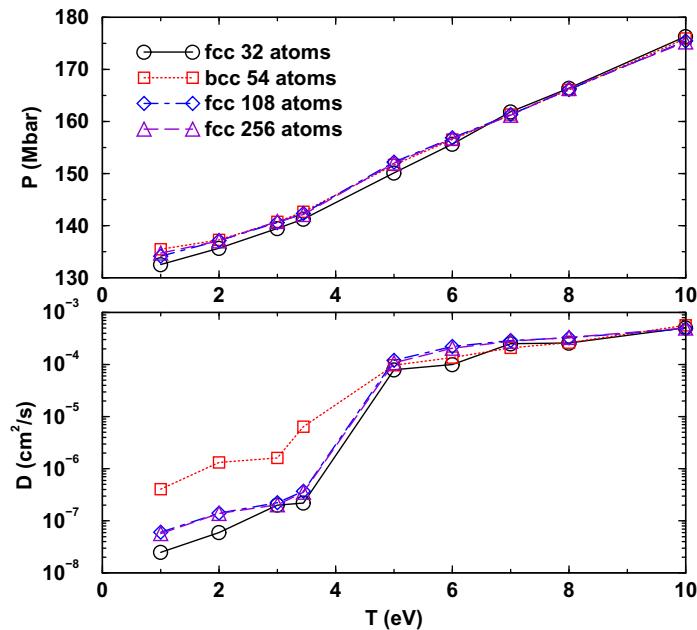


**Figure 1.** Size effect on the pressure (upper panel) and diffusion coefficient (lower panel) of Fe at  $45 \text{ g cm}^{-3}$ .

### 3. Convergence tests

For calculating the transport properties from first principles a number of atoms should be tested, since diffusion and viscosity are strongly dependent on the system sizes. For this purpose, in QLMD simulations, we tested face-centered cubic (fcc) structures with 32, 108 and 256 atoms and a body-centered cubic (bcc) structure with 54 atoms in a supercell at  $45 \text{ g cm}^{-3}$ . The pressure and diffusion versus temperature relations with different numbers of atoms are shown in figure 1. It is concluded that the pressure is not incredibly sensitive to the system sizes. In particular, the pressures are closer for different sizes when the temperatures are higher. The small difference at low temperatures may be caused by the long ranged orders with crystal structures. It is worth noting that the initial configurations of bcc and fcc structures are important for calculating diffusion in the solid phases, but the differences from different initial configurations disappear gradually with the increasing temperatures in the liquid phases (here above 5 eV).

According to the tests, it can be stated that our systems are in fact convergent for the calculation of pressure and diffusion coefficients when we use 108 atoms with initial fcc structures. It should be noted that when the system becomes liquid (after the jump in the diffusion coefficient), the results of 54 atoms, 108 atoms and 256 atoms are consistent. The difference at low temperatures would be from the different initial structures of bcc or fcc crystals. In fact, the small differences from different sizes can also come from the statistical errors for small sizes. Basically, this error can be overcome by longer time simulations.

For the viscosity, the results of the convergent tests are shown in figure 2. It is only useful for the liquids here since the viscosity is very large for solids. Here, the liquid phases are shown above 5 eV in our simulations. By comparison, we can know that the viscosity is incredibly sensitive to the sizes. For a small size of 32 atoms, the statistical errors are really large, which is not likely to be compensated by increasing the simulation time. When the number of atoms

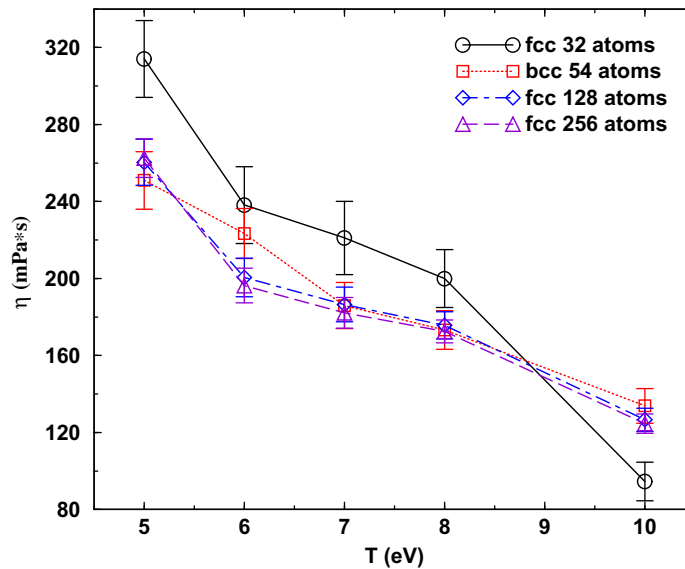


**Figure 2.** Size effect on the viscosity of Fe at  $45 \text{ g cm}^{-3}$  from QLMD simulations.

is increased up to 108 and 256, the viscosities at different temperatures seem convergent. Therefore, we can safely use the 108 atoms for the calculations of pressure, diffusion and viscosity in our cases. In fact, about 100 or 200 atoms are usually used in QMD simulations for the transport properties [8, 10, 12, 29–31], which has been shown to be convergent within reasonable errors.

For the effect of the particle number, we use a large number of particles up to 5324 in AAMD calculations to verify the convergence, as shown in figure 3. The simulation time is up to 100 ps in each case in order to obtain the correct correlations of particles in these semiclassical calculations. It can be shown that although the number of particles can affect the convergence of diffusion and viscosity, all the differences are within 10% or smaller. When the number reaches 4000, the diffusion and viscosity are almost convergent. In order to compare the results, we use 4000 particles in AAMD to calculate the transport properties below. It is worth noting that AAMD adopted pair potentials, which should be more sensitive to the size and debatable for the viscosity since the unsymmetrical shear of the system can not be described well by pair potentials.

For the density of  $33.385 \text{ g cm}^{-3}$ , we used 54 atoms with initial bcc structures to calculate their transport properties. The simulation details are also the same as those of  $45 \text{ g cm}^{-3}$ . Basically, the solid phase of Fe at  $33.385 \text{ g cm}^{-3}$  may be hexagonal close-packed (hcp). However, determining the lattice constants of hcp at high temperatures is very difficult; the dynamic properties such as the structure and melting behavior are very similar to the bcc structures [7, 45]. Therefore, we used bcc structures as the initial configurations. In fact, from the tests of Fe at  $45 \text{ g cm}^{-3}$ , it is now known that the transport properties are independent of the initial configurations when Fe melts. Furthermore, the effects of larger system sizes on calculated viscosities have been previously studied for models such as hard-sphere and Lennard–Jones liquids [44], showing meaningful values for  $\mu$  even with only 32 atoms. Thus, the initial configurations and sizes in this work can promise the reasonable accuracy of our simulations.

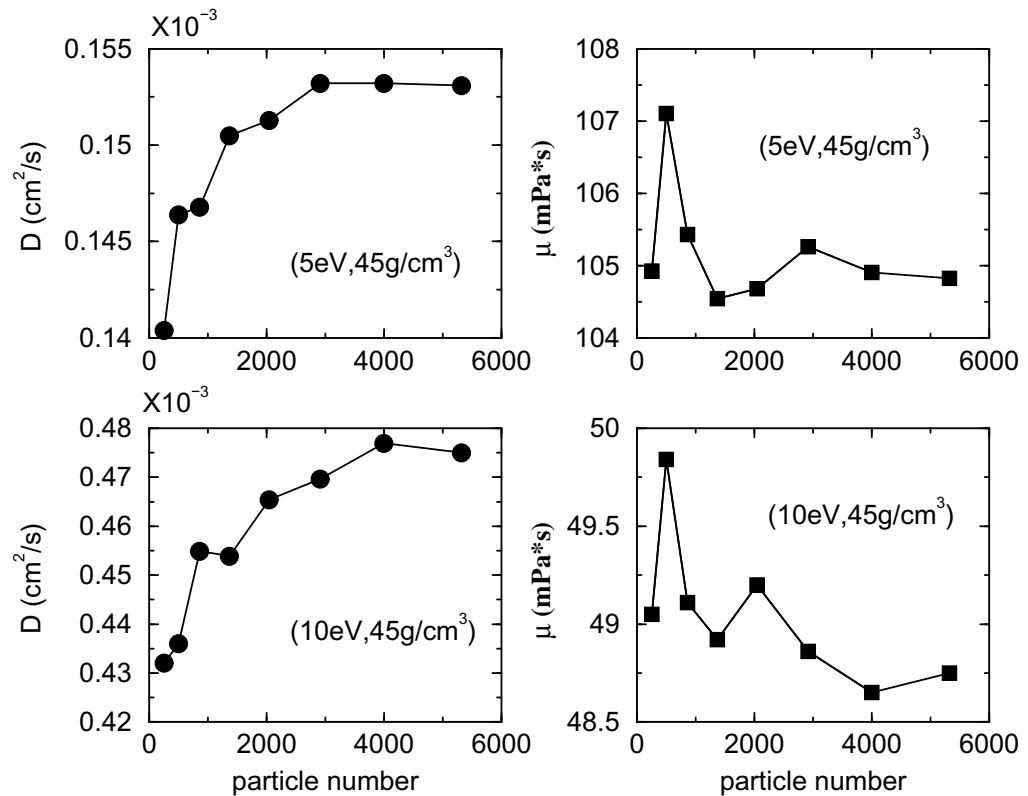


**Figure 3.** Size effect on the viscosity of Fe at  $45 \text{ g cm}^{-3}$  from AAMD simulations.

#### 4. Structural dynamics

The dynamic structures for dense matter are basic when attempting to understand the melting behaviors and the dynamics in a planet's core. However, dense liquid Fe has rarely been studied before due to the lack of effective methods. Dense Fe can hold the solid phase or ordered structures at very high temperatures, form clusters and chemical bonds assisted by core electrons [18] and keep a high melting temperature [45–47]. Here, the structures are investigated by looking at the radial distribution functions (RDF)  $g(r)$ , as shown in figures 4 and 5.

From the RDF, we can know that when the temperature increases up to 5 eV, Fe exhibits liquid behaviors at  $45 \text{ g cm}^{-3}$  and above 3 eV at  $33.385 \text{ g cm}^{-3}$ . We calculated the details of the dynamic structures near 5 and 3 eV for the two densities respectively, using the two phase approach [45] with 216 atoms and 108 atoms to obtain the melting temperature. The melting temperatures are found to be around 57 000 and 30 000 K, within the errors of 200 K in our simulations. The same behaviors can also be found in the data of diffusion coefficients and viscosities, which are shown in figures 1 and 2 and will be discussed in detail later. In this stage, the Fe at  $45 \text{ g cm}^{-3}$  and 40 000 K is also in the solid phase in the Fe phase diagram [7].

We should note that the first peaks of the RDF move toward to the zero point, indicating that the effective distance between ions decreases with the increasing temperatures. Therefore, we may use the positions of the first peaks in the RDF as the effective atomic diameters when discussing the SE relation later. If we use only the averaged ionic radius, the temperature effect

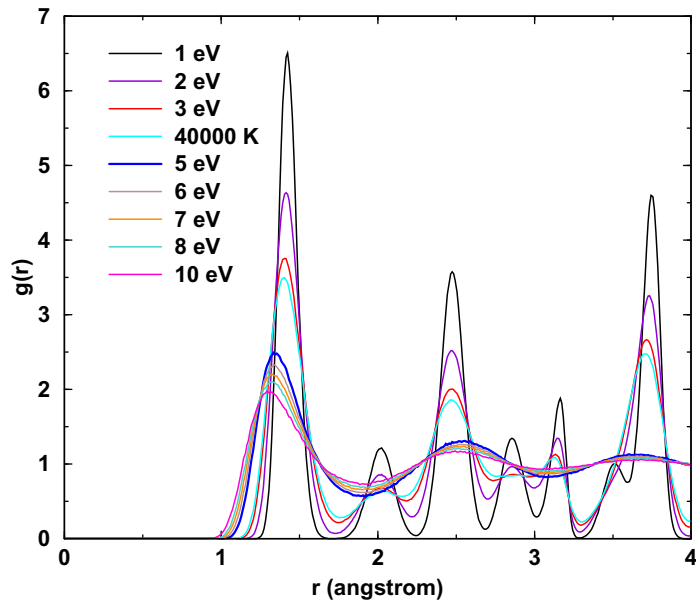


**Figure 4.** RDF versus temperature for Fe at  $45 \text{ g cm}^{-3}$ .

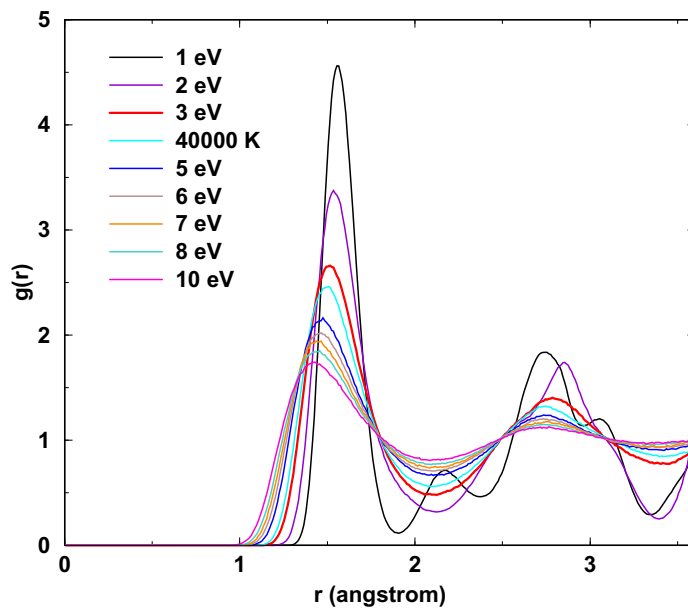


**Figure 5.** RDF versus temperature for Fe at  $33.385 \text{ g cm}^{-3}$ .

cannot be included since the radius is only dependent on the type of elements and system densities.

## 5. Transport properties

After the convergence tests, we can obtain the transport properties including EOS, diffusion coefficients and viscosities for dense Fe. The summaries of the data are shown in tables 1 and 2.

**Table 1.** Summary of the results of dense Fe at different temperatures at  $45 \text{ g cm}^{-3}$ .  $D^R$  and  $D^V$  are respectively defined in equations (1) and (2).  $D_{\text{AAMD}}$  and  $\mu_{\text{AAMD}}$  are the diffusion coefficient and viscosity from AAMD calculations, respectively.

$T$ (eV)	$P$ (Mbar)	$D^R$ ( $\text{cm}^2 \text{ s}^{-1}$ )	$D^V$ ( $\text{cm}^2 \text{ s}^{-1}$ )	$\mu$ (mPa s)	$P_{\text{AAMD}}$ (Mbar)	$D_{\text{AAMD}}$ ( $\text{cm}^2 \text{ s}^{-1}$ )	$\mu_{\text{AAMD}}$ (mPa s)
1	134.128	$0.61 \times 10^{-7}$	$0.60 \times 10^{-7}$	–	245.13	$2.39 \times 10^{-8}$	–
2	137.148	$1.40 \times 10^{-7}$	$1.61 \times 10^{-7}$	–	250.25	$9.55 \times 10^{-8}$	–
3	140.594	$2.24 \times 10^{-7}$	$2.68 \times 10^{-7}$	–	255.73	$2.07 \times 10^{-7}$	–
3.447	142.295	$3.72 \times 10^{-7}$	$3.82 \times 10^{-7}$	–	258.11	$2.91 \times 10^{-7}$	–
5	152.218	$1.21 \times 10^{-4}$	$1.23 \times 10^{-4}$	$62.07 \pm 6$	270.77	$1.54 \times 10^{-4}$	104.29
6	156.825	$2.22 \times 10^{-4}$	$2.11 \times 10^{-4}$	$44.11 \pm 5$	275.11	$2.11 \times 10^{-4}$	83.38
7	161.296	$3.15 \times 10^{-4}$	$3.05 \times 10^{-4}$	$41.29 \pm 4$	279.43	$2.73 \times 10^{-4}$	69.47
8	166.081	$3.26 \times 10^{-4}$	$3.37 \times 10^{-4}$	$38.13 \pm 4$	283.65	$3.39 \times 10^{-4}$	60.34
10	175.421	$4.86 \times 10^{-4}$	$4.83 \times 10^{-4}$	$27.72 \pm 3$	292.46	$4.77 \times 10^{-4}$	48.64

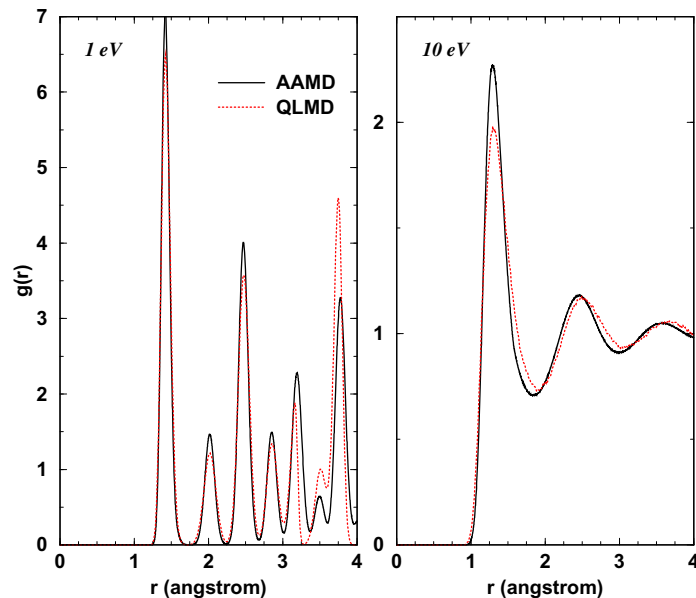
In the tables, pressures and diffusion coefficients from AAMD are also shown. When the solid phases are not broken, the diffusion coefficients are very small and the viscosities are very large (therefore they are not convergent in the Green–Kubo equation).

For a density of  $45 \text{ g cm}^{-3}$ , from table 1, the diffusion coefficients change rapidly between the temperatures of 40 000 K (3.447 eV) and 5 eV, and reach the orders of liquids diffusion at 5 eV. Also, the viscosities above 5 eV go to convergence when we integrate the pressure autocorrelations in equation (3), indicating the existence of liquid phases. However, AAMD gives the liquid Fe at 4 eV (not shown here), showing its limitations from pair potentials in very strongly coupling regimes. Furthermore, we can see that the diffusion coefficients from equations (1) and (2) are equal, which shows the validation and convergence of our simulations. For the pressure, AAMD gives much larger pressures than those of QLMD simulations, which is caused by the electronic structure calculations from Thomas–Fermi methods. It is very interesting that when the temperatures are above 5 eV, the diffusion coefficients from QLMD and AAMD are very close. One reason might be that the diffusion coefficients are strongly dependent on the nearest neighbor distributions. Pair potentials can deal with the nearest neighbor interactions between ions with good accuracy. This can be verified using the comparisons of RDF from QLMD and AAMD, as shown in figure 6, where the positions of the first peaks of RDF are almost overlapped. Therefore, the nearest neighbor interactions should be reasonable in AAMD. However, AAMD cannot deal with many-body interactions, suggesting that the shear viscosities from AAMD are incorrect here, since dense Fe liquid holds a lot of medium ordered structures; therefore, the melting behavior is not correct within the AAMD framework.

For a density of  $33.385 \text{ g cm}^{-3}$ , the behaviors are almost the same. The melting temperature locates below 3 eV, according to the RDF and diffusion coefficients. It is noted that the pressures from AAMD are much closer to those from QLMD compared with the results of  $45 \text{ g cm}^{-3}$ . This means that the electronic structures from the AA model are reasonable here but give more free electrons at  $45 \text{ g cm}^{-3}$ . Furthermore, the melting temperature from AAMD is also lower than that from QLMD; the diffusion coefficients are in the same order when Fe melts above 3 eV.

**Table 2.** Summary of the results of dense Fe at different temperatures at  $33.385 \text{ g cm}^{-3}$ .

$T$ (eV)	$P$ (Mbar)	$D^R$ ( $\text{cm}^2 \text{ s}^{-1}$ )	$D^V$ ( $\text{cm}^2 \text{ s}^{-1}$ )	$\mu$ (mPa s)	$P_{\text{AAMD}}$ (Mbar)	$D_{\text{AAMD}}$ ( $\text{cm}^2 \text{ s}^{-1}$ )	$\mu_{\text{AAMD}}$ (mPa s)
1	60.547	$3.50 \times 10^{-7}$	$3.21 \times 10^{-7}$	–	79.52	$2.11 \times 10^{-6}$	–
2	63.471	$2.45 \times 10^{-6}$	$2.19 \times 10^{-6}$	–	84.05	$2.69 \times 10^{-5}$	–
3	67.739	$6.70 \times 10^{-5}$	$6.71 \times 10^{-5}$	$47.1996 \pm 5$	86.99	$1.49 \times 10^{-4}$	29.43
3.447	69.786	$1.16 \times 10^{-4}$	$1.14 \times 10^{-4}$	$40.3466 \pm 5$	88.36	$1.84 \times 10^{-4}$	27.32
5	75.282	$2.98 \times 10^{-4}$	$2.85 \times 10^{-4}$	$24.217 \pm 3$	92.57	$3.28 \times 10^{-4}$	22.39
6	79.727	$3.67 \times 10^{-4}$	$3.74 \times 10^{-4}$	$19.8484 \pm 2$	95.33	$4.15 \times 10^{-4}$	20.41
7	82.248	$5.99 \times 10^{-4}$	$5.91 \times 10^{-4}$	$18.1716 \pm 2$	98.30	$5.08 \times 10^{-4}$	19.00
8	85.825	$6.08 \times 10^{-4}$	$5.98 \times 10^{-4}$	$17.1372 \pm 2$	101.11	$6.13 \times 10^{-4}$	17.83
10	93.098	$7.51 \times 10^{-4}$	$7.69 \times 10^{-4}$	$15.7396 \pm 2$	107.30	$8.01 \times 10^{-4}$	16.28

**Figure 6.** RDF comparison between AAMD and QLMD for Fe at  $45 \text{ g cm}^{-3}$ .

The small sizes in the calculations can introduce statistical errors. Especially for the viscosities, the errors are within 10%. Therefore, calculations with more than 10 000 atoms at least and accurate many-body potentials are needed basically. We need to construct more accurate semiclassical potentials for obtaining more accurate diffusion coefficients and viscosities.

## 6. Stokes–Einstein relation

With respect to the simulation time and system sizes, we find that the diffusion coefficients can reach convergence much more easily than the viscosities. Therefore, if we can obtain viscosities from calculated diffusions, a lot of computational resources can be saved. Therefore,

**Table 3.** Summary of the effective diameters and their corresponding viscosities for dense Fe at different temperatures at  $45 \text{ g cm}^{-3}$ .  $\bar{Z}$  is the average ionization degree from AA calculations.  $\mu_i$ ,  $\mu_f$  and  $\mu_E$  are the viscosities corresponding to different definitions of effective atomic diameters of ions  $r_i$ ,  $r_f$  and  $r_E$ , respectively.  $\mu_{\text{YVM}}$  is the viscosity from the Yukawa viscosity model (YVM) (see details in [14]).

$T$ (eV)	$r_i$ (Å)	$\mu_i$ (mPa s)	$r_f$ (Å)	$\mu_f$ (mPa s)	$r_E$ (Å)	$\mu_E$ (mPa s)	$\bar{Z}$	$\mu_{\text{YVM}}$ (mPa s)
5	1.275	83.361	1.335	79.612	1.338	79.428	13.011	43.99
6	1.275	54.002	1.330	51.767	1.323	52.052	13.009	37.97
7	1.275	46.527	1.325	44.770	1.309	45.302	13.009	33.77
8	1.275	49.051	1.320	47.377	1.297	48.219	13.002	30.71
10	1.275	41.166	1.295	40.529	1.276	41.127	12.993	26.64

the validation of the SE relation is important and meaningful. In order to test the validation, we calculate viscosities from different definitions of effective atomic diameters: averaged ionic distance at a specific density  $r_i = V^{(1/3)}$  (where  $V$  is the averaged volume of one atom at a specific density), the position of the first peaks in RDF ( $r_f$ ) and the effective radius ( $r_E$ ) from effective coordination number (ECN) definition. ECN can reveal the topology of the structures partly and can also give the local information around one atom. The definition of ECN is as follows:

$$\text{ECN} = \frac{1}{N} \sum_{i=1}^N \text{ECN}_i = \frac{1}{N} \sum_{i=1}^N \sum_{j \neq i} \exp \left[ 1 - \left( \frac{d_{ij}}{d_{\text{av}}^i} \right)^6 \right], \quad (5)$$

where  $d_{ij}$  is the distance between atoms  $i$  and  $j$ ;  $N$  is the total number of atoms in the system;  $d_{\text{av}}^i$  and its average value  $d_{\text{av}}$  are defined as

$$d_{\text{av}}^i = \frac{\sum_j d_{ij} \exp \left[ 1 - \left( \frac{d_{ij}}{d_{\text{av}}^i} \right)^6 \right]}{\sum_j \exp \left[ 1 - \left( \frac{d_{ij}}{d_{\text{av}}^i} \right)^6 \right]}, \quad d_{\text{av}} = \frac{1}{N} \sum_{i=1}^N d_{\text{av}}^i. \quad (6)$$

With this definition, the effective diameters  $r_E = d_{\text{av}}$ , which includes the temperature and density effects.

The results of different effective atomic diameters and the calculated viscosities from the SE relation are shown in tables 3 and 4. Comparing the results with the calculated viscosities from the Green–Kubo equation, we find that the viscosities are very different at low temperatures. With the increasing temperature, the SE relation seems to be more and more validated. Moreover, the choice of the effective atomic diameters plays an important role in the validation of the SE relation, where definitions of the positions of the first peaks of RDF and diameters from ECN calculations are more appropriate. Considering the calculation uncertainties and statistical errors, the SE relations can be considered validated only when the choice of the effective diameters are reasonable.

In order to avoid using the SE relation, some models have been constructed. For example, Murrilo reported the construction of the YVM based on molecular dynamics simulations [14],

**Table 4.** Summary of the effective diameters and their corresponding viscosities for dense Fe at different temperatures at  $33.385 \text{ g cm}^{-3}$ .

$T$ (eV)	$r_i$ (Å)	$\mu_i$ (mPa s)	$r_f$ (Å)	$\mu_f$ (mPa s)	$r_E$ (Å)	$\mu_E$ (mPa s)	$\bar{Z}$	$\mu_{\text{YVM}}$ (mPa s)
3	1.408	81.002	1.515	75.301	1.488	76.667	9.344	28.65
3.447	1.408	53.831	1.505	50.375	1.473	51.459	9.343	25.81
5	1.408	30.300	1.475	28.931	1.437	29.687	9.332	20.23
6	1.408	29.633	1.465	28.488	1.419	29.410	9.326	18.41
7	1.408	21.147	1.455	20.469	1.404	21.214	9.323	17.28
8	1.408	23.847	1.450	23.162	1.388	24.197	9.312	16.56
10	1.408	24.122	1.425	23.840	1.364	24.912	9.296	15.91

which can be used in a warm dense regime. We verify the validation of the YVM model here. First of all, we give the average ionization degree ( $\bar{Z}$ ) from the AA model with electronic energy-level broadening [22] and then show the viscosities ( $\mu_{\text{YVM}}$ ) from the YVM model, as shown in tables 3 and 4. It can be shown that the YVM model improves the accuracy of the SE relation, especially for cases at high temperatures. This suggests that the Yukawa potential might be reasonable for states at such high densities and at relatively high temperatures.

What is the possible reason for the debatable validation of the SE relation in this regime? The basic physics is whether the ions exhibit as Brownian particles. For the specific case in this work, heavy Fe ions move in the liquid-like electron sea and randomly collide with many free-like electrons. However, the other dominant factor for ionic motions is the interactions between ions, i.e. the strong coupling of ions. Every ion moves in a specific force field determined by both electrons and ions; this force field is not constant. The ions in dense matter have a memory effect, i.e. the ionic positions at this time play an important role in the ionic movements the next time. In other words, if the correlation time of ions is larger than the observable time, the motion of the ions should not have a Markov process. In order to analyze the correlation time of the systems, the velocity autocorrelation functions (VAF) of ions at 5 and 10 eV are shown in figure 7. Here, we adopt the simplest definition of the correlation time ( $\tau_c$ ) to compare the correlation time at different temperatures. Here,  $\tau_c$  is defined as the time for which the VAF( $t$ ) decreases to  $1/e$  [48]. With this definition,  $\tau_c$  is about 4.1 and 2.7 fs for the temperatures of 5 and 10 eV, respectively. Therefore, with the increasing temperature, the behaviors of ions have a more and more Brownian-like motion. In fact, if the system is ideal gas, the correlation time will be zero, indicating uncorrelated behaviors between two near time steps. That is to say, when the temperature is high enough, the random collisions between particles are dominant and the statistical behaviors can work well. If the correlation time of the system is zero, we can recover the SE relation directly from equations (2) and (3) [49]. We can then conclude that the SE relation is strongly dependent on the coupling parameters of ions  $\Gamma = Z^{*2}/(k_B T a)$ , with  $T$  the system temperature,  $k_B$  the Boltzmann constant,  $a$  the mean ionic sphere radius defined as  $a = (3/(4\pi n_i))^{1/3}$ ,  $Z^*$  the average ionization degree and  $n_i$  the ionic number density. If  $\Gamma$  is small enough, the SE relation can be valid. Furthermore, one possible reason that QMD or QLMD can obtain reasonable transport properties within a relatively short time (within 10 ps) is the short correlation time of particles, as shown in figure 7.

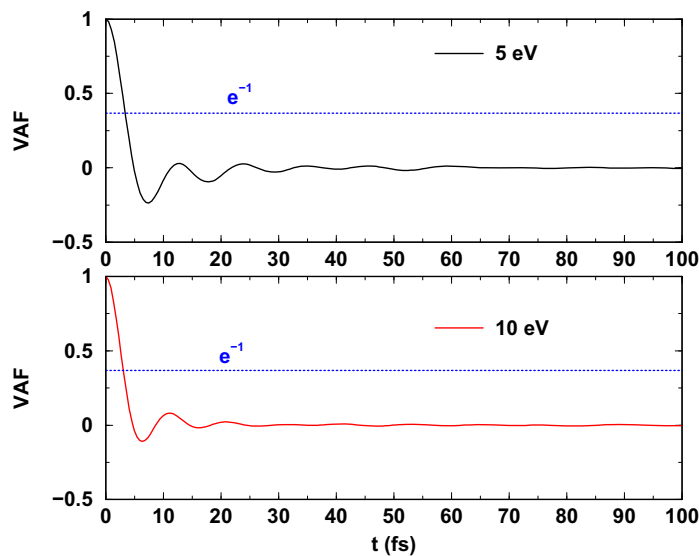


**Figure 7.** Velocity autocorrelation function (VAF) of Fe ions at the temperatures of 5 eV (upper panel) and 10 eV (lower panel) from QLMD calculations for Fe at  $45 \text{ g cm}^{-3}$ .

## 7. Conclusion

In conclusion, the dynamic structures and transport properties including EOS, diffusion and viscosities are calculated using the QLMD method within the framework of first principles. The dynamic structures provide information about RDF, melting behaviors, diffusions and viscosities. The validation of the SE relation is also discussed, showing the importance of the methods of choosing the effective atomic diameters. This work studies the dense liquid Fe existing in giant planets such as Jupiter and exoplanets, indicating the necessity of first principles calculations or constructing accurate many-body interactions. Furthermore, the results are crucial for understanding laser-shock induced compression experiments, reminding us of the complexity of dense matter. In this field, a great deal of new physics needs to be studied to a greater depth.

## Acknowledgments

This work was supported by the National NSFC under grant numbers 11104351, 11274383, 60921062, 11005153 and 11104350. Calculations are carried out at the Research Center of Supercomputing Application, NUDT.

## References

- [1] Swift D C *et al* 2012 Mass-radius relationships for exoplanets *Astrophys. J.* **744** 59
- [2] Jin F T *et al* Radiative opacity of iron studied using a detailed level accounting model *Astrophys. J.* **693** 597–609
- [3] Gao C and Zeng J L 2008 Spectrally resolved and Rosseland and Planck mean opacities of iron plasmas at temperatures above 100 eV: a systematic study *Phys. Rev. E* **78** 046407

- [4] Moses E I *et al* 2009 The National Ignition Facility: Ushering in a new age for high energy density science *Phys. Plasmas* **16** 041006
- [5] Jeanloz R *et al* 2007 Achieving high-density states through shock-wave loading of precompressed samples *Proc. Natl Acad. Sci. USA* **104** 9172–7
- [6] Pickard C J and Needs R J 2009 Stable phases of iron at terapascal pressures *J. Phys.: Condens. Matter* **21** 452205
- [7] Stixrude L 2012 Structure of iron to 1 Gbar and 40 000 K *Phys. Rev. Lett.* **108** 055505
- [8] Wijs Gilles A *et al* 1998 The viscosity of liquid iron at the physical conditions of the Earth's core *Nature* **392** 805
- [9] Alfè D, Gillan M J and Price D G 1999 The melting curve of iron at the pressures of the Earth's core from *ab initio* calculations *Nature* **401** 462
- [10] Alfè D and Gillan M J 1998 First-principles calculation of transport coefficients *Phys. Rev. Lett.* **81** 5161
- [11] Alfè D and Gillan M J 1998 First-principles simulations of liquid Fe–S under Earth's core conditions *Phys. Rev. B* **58** 8248
- [12] Vočadlo L, Alfè D, Price G D and Gillan M J 2000 Transport coefficients of liquids from first principles *Phys. Earth Planet. Inter.* **120** 145
- [13] Saigo T and Hamaguchi S 2002 Shear viscosity of strongly coupled Yukawa systems *Phys. Plasmas* **9** 1210–6
- [14] Murillo M S 2008 Viscosity estimates of liquid metals and warm dense matter using the Yukawa reference system *High Energy Density Phys.* **4** 49–57
- [15] Daligault J 2012 Diffusion in ionic mixtures across coupling regimes *Phys. Rev. Lett.* **108** 225004
- [16] Ma Y M *et al* 2009 Transparent dense sodium *Nature* **458** 182
- [17] Pickard C J and Needs R J 2010 Aluminium at terapascal pressures. *Nature Mater.* **9** 624–27
- [18] Dai J Y *et al* 2011 Dynamic ionic clusters with flowing electron bubbles from warm to hot dense iron along the Hugoniot curve *Phys. Rev. Lett.* **109** 175701
- [19] Dai J Y, Hou Y and Yuan J M 2010 Unified first principles description from warm dense matter to ideal ionized gas plasma: electron–ion induced friction *Phys. Rev. Lett.* **104** 245001
- [20] Dai J Y, Hou Y and Yuan J M 2010 Quantum Langevin molecular dynamics determination of the solar-interior equation of state *Astrophys. J.* **721** 1158–63
- [21] Yuan J M 2002 Self-consistent average-atom scheme for electronic structure of hot and dense plasmas of mixture *Phys. Rev. E* **66** 047401
- [22] Hou Y, Jin F T and Yuan J M 2006 Influence of the electronic energy level broadening on the ionization of atoms in hot and dense plasmas: an average atom model demonstration *Phys. Plasmas* **13** 093301 and references therein
- [23] Mazevet S, Lambert F, Bottin F, Zérah G and Clérouin J 2007 *Ab initio* molecular dynamics simulations of dense boron plasmas up to the semiclassical Thomas–Fermi regime *Phys. Rev. E* **75** 056404
- [24] Lambert F, Clérouin J and Zérah G 2006 Very-high-temperature molecular dynamics *Phys. Rev. E* **73** 016403
- [25] Danel J-F, Kazandjian L and Zérah G 2012 Numerical convergence of the self-diffusion coefficient and viscosity obtained with Thomas–Fermi–Dirac molecular dynamics *Phys. Rev. E* **85** 066701
- [26] Mermin N D 1965 Thermal properties of the inhomogeneous electron gas *Phys. Rev.* **137** A1441–3
- [27] Graziani F R *et al* 2012 Large-scale molecular dynamics simulations of dense plasmas: the Cimarron project *High Energy Density Phys.* **8** 105–31
- [28] Dai J Y, Hou Y and Yuan J M 2011 Influence of ordered structures on electrical conductivity and XANES from warm to hot dense matter *High Energy Density Phys.* **7** 84–7
- [29] Kress J D, Cohen James S, Horner D A, Lambert F and Collins L A 2010 Viscosity and mutual diffusion of deuterium–tritium mixtures in the warm-dense-matter regime *Phys. Rev. E* **82** 036404
- [30] Horner D A, Lambert F, Kress J D and Collins L A 2009 Transport properties of lithium hydride from quantum molecular dynamics and orbital-free molecular dynamics *Phys. Rev. B* **80** 024305
- [31] Lambert F and Recoules V 2012 Plastic ablator and hydrodynamic instabilities: a first-principles set of microscopic coefficients *Phys. Rev. E* **86** 026405

- [32] Kress J D *et al* 2011 Quantum molecular dynamics simulations of transport properties in liquid and dense-plasma plutonium *Phys. Rev. E* **83** 026404
- [33] Dai J Y and Yuan J M 2009 Large scale efficient Langevin dynamics and why it works *Europhys. Lett.* **88** 20001
- [34] Giannozzi P *et al* 2009 Quantum ESPRESSO: a modular and open-source software project for quantum simulations of materials *J. Phys.: Condens. Matter* **21** 395502
- [35] Perdew J P, Burke K and Ernzerhof M 1996 Generalized gradient approximation made simple *Phys. Rev. Lett.* **77** 3865–8
- [36] Zhang H L *et al* 2010 Static equation of state of bcc iron *Phys. Rev. B* **82** 132409
- [37] Hou Y and Yuan J M 2009 Alternative ion–ion pair-potential model applied to molecular dynamics simulations of hot and dense plasmas: Al and Fe as examples *Phys. Rev. E* **79** 016402
- [38] Allen M P and Tildesley T J 1987 *Computer Simulation of Liquids* (Oxford: Clarendon)
- [39] Collins L, Kwon I, Kress J, Troullier N and Lynch D 1995 Quantum molecular dynamics simulations of hot, dense hydrogen *Phys. Rev. E* **52** 6202–19
- [40] Mithen J P, Daligault J and Gregori G 2012 Molecular dynamics simulations for the shear viscosity of the one-component plasma *Contrib. Plasma Phys.* **52** 58–61
- [41] Lorenzen W, Holst B and Redmer R 2009 Demixing of hydrogen and helium at megabar pressures *Phys. Rev. Lett.* **102** 115701
- [42] Plagemann K U *et al* 2012 Dynamic structure factor in warm dense beryllium *New J. Phys.* **14** 055020
- [43] Cappelezzo M, Capellari C A, Pezzin S H and Coelho L A F 2007 Stokes–Einstein relation for pure simple fluids *J. Chem. Phys.* **126** 224516
- [44] Schoen M and Hoheisel C 1985 The shear viscosity of a Lennard–Jones fluid calculated by equilibrium molecular dynamics *Mol. Phys.* **56** 653–72
- [45] Morard G, Bouchet J, Valencia D, Mazevet S and Guyot F 2011 The melting curve of iron at extreme pressures: implications for planetary cores *High Energy Density Phys.* **7** 141–4
- [46] Nguyen Jeffrey H and Holmes Neil C 2004 Melting of iron at the physical conditions of the Earth’s core *Nature* **427** 339–42
- [47] Alfè D 2009 Temperature of the inner-core boundary of the earth: melting of iron at high pressure from first-principles coexistence simulations *Phys. Rev. B* **79** 060101
- [48] Kesselring T A, Franzese G, Buldyrev S V, Herrmann H J and Stanley H E 2012 Nanoscale dynamics of phase flipping in water near its hypothesized liquid–liquid critical point *Sci. Rep.* **2** 474
- [49] Frenkel D and Smit B 1996 *Understanding Molecular Simulation* (San Diego, CA: Academic)